

# THE CONTRIBUTION OF DWARF PLANETS TO THE ORIGIN OF LOW INCLINATION COMETS BY THE REPLENISHMENT OF MEAN MOTION RESONANCES IN DEBRIS DISKS.

M. A. MUÑOZ-GUTIÉRREZ

Institute of Astronomy and Astrophysics, Academia Sinica, National Taiwan University, Taipei, Taiwan

A. PEIMBERT AND B. PICHARDO.

Instituto de Astronomía, Universidad Nacional Autónoma de México, Apdo. postal 70-264 Ciudad Universitaria, México

*Accepted for publication in the A.J.*

## ABSTRACT

In this work we explore a new dynamical path for the delivery of low-inclination comets. In a configuration formed by an interior giant planet and an exterior massive debris disk, where the mass is accounted for by the 50 largest objects in the disk, the strongest mean motion resonances of the giant, located along the belt, are replenished with new material (test particles) due to the influence of the 50 massive objects. Once in resonance, slow chaotic diffusion stirs the orbital elements of the cometary nuclei enough to encounter the giant and to be scattered by it. When the disk is massive enough, both resonant and non-resonant particles are stirred quickly to encounter the giant and form a scattered disk component, greatly increasing the rate for the delivery of cometary material to the inner part of the system. This mechanism is applicable both to the solar system and extrasolar systems in general. Preliminary results, using a disk as massive as the classical Kuiper belt, indicate that the mechanism here proposed can account for about a tenth of the required injection rate to maintain the population of ecliptic comets in steady state. In a more massive belt of  $0.25 M_{\oplus}$ , an estimated rate of around 0.6 new comets per year is found. Such a high rate would pose a serious risk for the habitability of rocky interior planets, yet would resemble the late heavy bombardment that was present in the early solar system.

*Keywords:* planet-disk interactions — comets: general — methods: numerical

## 1. INTRODUCTION

Beyond the orbit of the outermost planet known of the solar system, a large reservoir of cometary nuclei, going from the trans-Neptunian region to the outer edge of the Oort cloud, fills the space up to an incredible distance of approximately 100,000 au. In there, thousands of millions of bodies coexist nearly in steady state. A few of these bodies however are destabilized every now and then producing one of the most staggering astrophysical phenomenologies: comets. A cometary nucleus becomes a comet (i.e. an icy body with a coma and a long tail produced by sublimation of mainly water ice by solar radiation) when its orbit is disrupted, advancing progressively towards the inner solar system, by increasing their eccentricity while reducing their perihelion distance (Dones et al. 2015, and references therein).

Although the Kuiper belt is far and away the best known cometary reservoir, there are hundreds of planetary systems with conspicuous debris disks or Kuiper belt like structures discovered in the last decade (Wyatt 2008; Matthews et al. 2014; Wyatt 2018); some examples of them are the ones circling Fomalhaut,  $\beta$ Pictoris, Vega, etc. Compared to those debris disks, our Kuiper belt is actually “anemic”, fortunately for life in the solar system. In spite of its low mass, its existence remains relevant for the inner parts of the solar system and much data has been collected about it. We present here a short overview of the information related to the topic introduced in this work. The solar system data presented below should also

be relevant for most extrasolar systems.

In the solar system, once cometary nuclei descend to the inner solar system, they become planet crossers and are exposed to continuous orbital perturbations that diminish swiftly their survival probabilities; this means that, given the current population of comets in the inner solar system, the most probable scenario is that cometary nuclei are continuously resupplied somehow from the trans-Neptunian region (Fernandez 1980; Duncan et al. 1988; Nesvorný et al. 2017).

An important endeavor has been done trying to explain the current number of comets, particularly the low inclination comets (or ecliptic comets). In an influential work, Levison & Duncan (1997), showed that in order to maintain a constant population of ecliptic comets (defined by the authors as those with a Tisserand parameter with respect to Jupiter of  $2 < T_J < 3$ ), the Kuiper belt objects with orbits that become Neptune’s crossers, could evolve into an orbit with perihelion smaller than 2.5 au, where they turn into active comets. In that work, the authors conclude that in order to explain the observed inclination distribution, the ecliptic comets would need to be active for a long time (about 12,000 years) after they have reached a 2.5 au perihelion distance.

A first scenario to explain the current population of ecliptic comets in the solar system is one where the resonant regions of the classical Kuiper belt are the suppliers (e.g. Morbidelli 1997; Tiscareno & Malhotra 2009). In that scenario, the gravitational effect of Neptune is considered as the only one exerted that produces the escape of bodies from the classical Kuiper belt (CKB), and

governs, by secular chaotic processes in its orbital resonances, the motion of cometary nuclei in the belt. The low efficiency of such process in this apparently highly stable environment, made researchers to come up with new interesting ideas of more efficient processes to explain the current population of low inclination comets in the inner solar system. Currently, there seems to be a general consensus that the classical Kuiper belt is not an important source of the ecliptic comets because of the extremely stable orbits of the cometary nuclei after Neptune stopped migrating. However, we will show in this work that once the effect of dwarf planets is considered, this scenario can supply a fraction, that under some circumstances might be significant, of the observed comets.

In a second scenario, the in-falling cometary nuclei originate in the scattered disk instead of in the CKB (Duncan & Levison 1997; Volk & Malhotra 2008). This scenario takes advantage of the fact that the scattered disk is far less stable than the classical belt, therefore it is a more efficient source of ecliptic comets because of their proximity to Neptune at perihelion (it is also a better source of Halley type comets Levison et al. 2006; Volk & Malhotra 2008; Nesvorný et al. 2017). Assuming the scattered disk is the main source of ecliptic and Halley type comets, estimates of the required number of cometary nuclei in the scattered disk (with diameters larger than  $\sim 2$  km) lie in the range  $1 - 6 \times 10^9$  objects (Levison et al. 2006; Brasser & Morbidelli 2013; Brasser & Wang 2015; Rickman et al. 2017). In this respect, although there are already some constraints, like, for instance, those based on occultation studies (Schlichting et al. 2009; Bianco et al. 2010), we do not have yet a definitive answer. Also, given the wider inclination distribution of cometary nuclei found in the scattered disk (median  $\sim 20 - 25^\circ$ ; Gulbis et al. 2010; Nesvorný et al. 2016), compared to the one of the ecliptic comets (median  $\sim 13^\circ$ ; Nesvorný et al. 2017), it is difficult to reconcile this scenario to explain the lowest inclination population of ecliptic comets (Rickman et al. 2017).

Nesvorný et al. (2017) present another approach to the solution of this problem by performing end-to-end simulations from the early stages of the solar system up to 4.5 Gyr (see also Nesvorný & Morbidelli 2012). Within this model, cometary nuclei reservoirs are formed since the early epochs of the solar system. The number of comets after 4.5 Gyr is proportional to the number of cometary nuclei in the original transplanetary disk, which can be calibrated based on the number of known Jupiter Trojans (Nesvorný & Vokrouhlický 2016), although recent results based on the color discrepancy between the Jupiter and Neptune Trojans sow doubts about a confident and direct relation between these populations and those in the Kuiper belt (Jewitt 2018). The authors conclude then that the main source of ecliptic comets is the scattered disk and the main source of Halley type comets is the Oort cloud.

Of course, although this detailed information and quantification of the comets statistics and direct observation has been up to now only conceivable in the solar system, the astounding discovery of comets in extrasolar planetary systems (e.g. Weaver et al. 1995; Movshovitz et al. 2012; Bodman & Quillen 2016; Rappaport et al. 2018; Wyatt et al. 2018), known now as exocomets, brings us to

an interesting epoch where dynamical studies of debris disks and the origin of exocomets will be closely studied and interpreted in a more statistical sense, as well as individually (including for instance, secular processes that bring comets to the interior regions of planetary systems).

In this work, we present a study that shows how the secular effect, produced by dwarf planets and minor bodies, on cometary nuclei (specifically on a classical Kuiper belt-like debris disk), becomes influential to the number of comets that descend to an inner planetary system. This mechanism brings cometary nuclei to the resonant regions in a continuous way that ensures an uninterrupted resupply of new comets; in the case of our solar system, this secular effect may be able to explain the origin of up to a fifth (or more) of the yet puzzling ecliptic comets.

This paper is organized as follows: in Section 2 we describe our debris disk models, the numerical simulations performed, and the result of a massless reference simulation. Section 3 is devoted to present and discuss the results for different disk masses, and the estimations for the in-falling rates of low-inclination comets in extrasolar systems (Sections 3.1, 3.2, 3.3, 3.4, and 3.6), including a toy model for the solar system as an example of application in subsection 3.5. Finally, in Section 4 we present our main conclusions.

## 2. METHODS AND SIMULATIONS

Our simulations were designed with the aim of demonstrating and characterizing the existence of the dynamical processes associated to a giant planet acting on an external debris disk; in this situation dwarf planet-sized objects sometimes play a crucial role on the secular evolution of the disk. While we are trying to study a broad set of physical parameters, in this work we select a toy model that loosely resembles the outer parts of the solar system (Neptune and the cold CKB). At the same time, this model will allow us to expand on it, in order to explore a broader sample of debris disks with giant and dwarf planets.

We recall that in order to study any specific example, like the solar system itself or any other extrasolar system, a detailed model accounting for the particular conditions of such system (like the mass of the star, mass of the disk, planetary architecture, etc.) would be required; however, such complexity is beyond the scope of the present paper.

In this study we demonstrate the existence of the phenomenology of the replenishment of mean motion resonances (MMRs) by dwarf-planet sized bodies (DPs), we present an initial characterization, as well as the need of a detailed modeling. We do this by obtaining order of magnitude estimates of its potential importance for our toy model of the solar system and for the most massive extrasolar scenarios at hand.

Each one of our simulations consists of a giant planet (equal to Neptune in all physical and orbital parameters, except for the inclination that was set to zero), 50 massive DPs, as well as 5000 test particles. All the simulations include a central star of  $1M_\odot$  and were performed by using the symplectic integrator contained in the MERCURY package of Chambers (1999), with an error tolerance of  $10^{-10}$  for the Bulirsch-Stöer integrator with an initial time-step of 180 days, for a total integration time

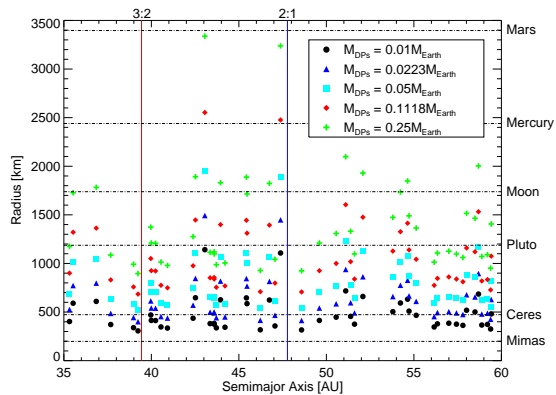


**Figure 1.** Spatial distribution of DPs vs. their size for different disk masses. The radius of each DP in the five different massive disks is plotted against its initial semimajor axis. Note that the spatial location is the same for each single DP, but they are just rescaled in mass to account for progressively more massive disks. The names and radius of six representative solar system bodies are indicated by the horizontal black dot-dashed lines and the labels at the right side of the plot. See text for details. Vertical lines mark the location of the 3:2 (red) and 2:1 (blue) MMRs with the giant planet.

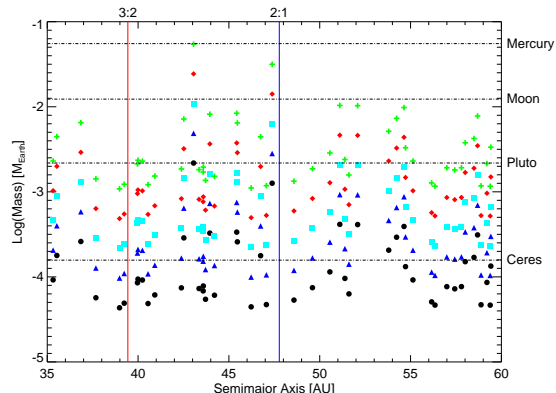


**Figure 2.** Spatial distribution of DPs vs. their mass for different disk total masses. The symbols and reference lines are the same as in Fig. 1. Note how our heaviest DP in the most massive disk is only as massive as Mercury despite being as large as Mars, due to the densities for icy bodies considered in this work.

of 1 Gyr.

### 2.1. Initial conditions for disk particles.

Our test particles, initially, are randomly distributed between 38 and 50 au forming a cold debris disk. The distributions of eccentricities and inclinations of the test particles were obtained from two sets of random gaussian distributions of points on a XY plane, from which we extract the eccentricity,  $e$ , and argument of periastron,  $\omega$ , in one case, and the inclination,  $i$ , and longitude of the ascending node,  $\Omega$ , on the other, as described in Muñoz-Gutiérrez et al. (2015). This method produces random gaussian distributions for  $e$  and  $i$ , with mean and standard deviations  $\langle e \rangle = 0.037$  and  $\sigma_e = 0.019$  for  $e$ , and  $\langle i \rangle = 1.52^\circ$  and  $\sigma_i = 0.80^\circ$  for  $i$ , respectively. At the same time  $\omega$  and  $\Omega$  are randomly distributed between 0 and  $360^\circ$ . Finally, the mean anomaly,  $M$ , is assigned randomly between 0 and  $360^\circ$ .

### 2.2. Initial conditions for the DP distributions.

The DPs are randomly distributed between 35 and 60 au, and they constitute the massive part of the debris disk, i.e., we assume the mass of the disk equals the added mass of the 50 DPs. Regarding the orbital distribution, all eccentricities and inclinations are randomly assigned between 0 and 0.1 and  $0^\circ$  and  $5^\circ$ , respectively, while the three angles,  $\omega$ ,  $\Omega$ , and  $M$ , are randomly assigned between  $0^\circ$  and  $360^\circ$ . The simulations shown in this work included some of those presented previously in Muñoz-Gutiérrez et al. (2017), plus several new cases.

In Muñoz-Gutiérrez et al. (2017) we demonstrated that the excitation levels of the disk particles are weakly dependent on the index of the DP differential mass distribution (dMD),  $\alpha$ . For a differential size distribution (dSD) of the form  $dN/dD \propto D^{-q}$ , a dMD will be given by:  $dN/dM \propto M^{-\alpha}$ , where  $\alpha$  is related to the index of the dSD,  $q$ , as  $\alpha = (2 + q)/3$ ; since, for a constant density,  $D \propto M^{1/3}$ . For disks in collisional equilibrium,  $\alpha \sim 1.8$  ( $q \sim 3.5$ ), while for the distribution of the largest Kuiper belt objects,  $\alpha \sim 2.2$  ( $q \sim 4.5$ ) (Dohnanyi 1969; Fraser et al. 2008; Fraser & Kavelaars 2008); based on this, throughout this work we make use of  $\alpha = 2$  for all our simulations (note that in Muñoz-Gutiérrez et al. 2017, we use an  $\alpha = 1.8$  for the experiments of Section 3.4).

We used debris disks of five different masses, as well as a massless case; the masses covered in this work are  $(\sqrt{5})^n \times 0.01M_\oplus$ , where  $n$  takes the values  $[0, 1, 2, 3, 4]$ ; for reference, estimates of the mass of the CKB vary between  $0.008M_\oplus < M_{CKB} < 0.06M_\oplus$  (Trujillo et al. 2001; Bernstein et al. 2004; Fuentes & Holman 2008; Vitense et al. 2010; Fraser et al. 2014). These masses correspond approximately to the range covered by our first three models.

Figs. 1 and 2 show the spatial distribution of all the DPs against their radius in km and mass in Earth masses, respectively. The radius of the DPs are calculated from their assigned random masses and densities. As we described in Muñoz-Gutiérrez et al. (2017), the mass of each DP,  $m_n$ , is assigned using the formula:

$$m_n = \left( \frac{K_\alpha}{(\alpha - 1)n'} \right)^{1/(1-\alpha)}. \quad (1)$$

where,  $\alpha = 2$ , while  $K_\alpha$  is a scaling constant related to the largest mass permitted in the distribution (e.g., for the  $0.01M_\oplus$  disk,  $K_\alpha$  is similar to the mass of Pluto). On the other hand, densities are randomly assigned between 1 and  $2.5 \text{ g cm}^{-3}$ , to cover the range from objects formed mainly by ice, to the denser dwarf planets in the solar system (Eris and Haumea; Barr & Schwamb 2016). In Fig. 1 we include six horizontal black dot-dashed lines that indicate the radius of six representative solar system bodies. Mimas is the smallest body in the solar system known to be round due to self-gravity, therefore by analogy, all of our objects, even in the less massive disk, would be spherical, even if they were composed by pure ice; the radius of Ceres imposes a limit for the proper recognition as dwarf planets (according to the current IAU criteria). Therefore, for our less massive disk, 19 of the objects in the distribution would be classified as dwarf planets, 39 in the  $0.0223M_\oplus$  disk, and all the 50 objects for the three most massive disks.

It can be seen from Figs. 1 and 2 that two objects are

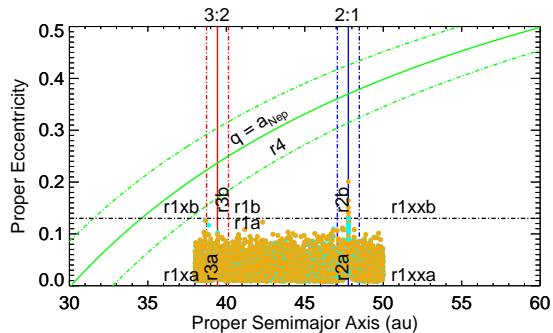


**Figure 3.** Initial and final distributions of proper elements for the reference simulation. We also show the different regions in the plane we have defined to track the evolution of particles. See text for details.

significantly more massive in each distribution than the rest of the DPs; these two objects will likely dominate the dynamics of the disk particles. It is worth to note that, for a disk of mass equal to  $0.01M_{\oplus}$ , these two objects are similar to Pluto, both in mass and size, while for the most massive disk ( $0.25M_{\oplus}$ ), those two objects are almost as large as Mars, but only as massive as Mercury (the density of both, Mercury and Mars, is much larger, approximately  $4\text{--}5\text{ g cm}^{-3}$ ), while the rest of the DPs range in size from a bit smaller than Pluto to a little larger than the Moon, while in mass most of them are only as massive as Pluto.

### 2.3. Reference simulation with a “zero-mass” disk.

The aim of this work is to explore the evolution of cometary nuclei, initially in the form of a cold debris disk, under the gravitational influence of an interior giant planet, and a distribution of DPs with different masses. In order to better understand the effect of DPs on the cometary nuclei on Gyr time scales, we first establish a point of reference by exploring the “zero-mass” disk case; i.e., a debris disk which contains only test particles (and no DPs) under the influence of a Neptune-like giant planet.

To analyze the evolution of test particles, throughout the paper we transform the osculating orbital elements ( $x(t')$ , where  $x$  represents  $a$ ,  $e$ , or  $i$ ) which constitute the usual output of our simulations, to proper orbital elements ( $x_p(t)$ ), namely: the proper semimajor axis,  $a_p$ , the proper eccentricity,  $e_p$ , and the proper inclination,  $i_p$ . The transformation is performed following the method described in Section 12.2 of Morbidelli (2002), such that:

$$x_p(t) = \frac{1}{N} \sum_{t'=t-5\text{Myr}}^{t'=t+5\text{Myr}} x(t'), \quad (2)$$

where  $N$  is the number of data points in the 10 Myr running window considered for the averaging procedure; this results in 100 data points of proper elements for each particle for the full 1 Gyr integration time span.

The result from the reference simulation is shown in Fig. 3, where cyan dots represent the first set of data points after the averaging procedure (this means they are not exactly equal to the osculating initial conditions of the test particles), while orange dots are the last set of data points, after 1 Gyr of evolution under the influence of the Neptune-like giant. In this phase-space plane of

proper orbital elements,  $a_p$  vs.  $e_p$ , we have defined several regions in order to track the evolution of particles:

First, we established a proper eccentricity limit,  $e_{lim}$ , below which all particles remain at the first data record of the proper elements for the reference simulation. This limit,  $e_{lim} = 0.13$ , is shown as a horizontal black dot-dashed line. Graphically, this limit separates five regions labeled as “a” (below the limit) from five regions labeled as “b” (above the limit). While physically, this limit separates particles that are mostly unaffected and that we consider to be cold, from those that have been already affected by the several bodies of the system, which we consider to be hot.

The second limit identifies particles that, after some evolutionary time, are thrown to a region where they are subjected to perturbations from the giant planet by close encounters. We define this limit by using the Hill radius of the giant,  $R_H = a_{gp}(M_p/3M_{\odot})^{1/3}$ , where  $a_{gp}$  and  $M_p$  are the semimajor axis and mass of the giant planet. Following Gladman & Duncan (1990); Bonsor & Wyatt (2012), we consider that a particle interacts with a planet once its periastron is inside the limits given by  $a_{gp} \pm 2\sqrt{3}R_H$ . The lines delimiting this region are shown in the plane  $a_p$  vs.  $e_p$  by the green dot-dashed lines. We also show the line of constant periastron equal to  $a_{gp}$  with a solid green line. Region 4 lies above the lower green dot-dashed line; particles in this region will be labeled as “crossers”. The importance of these particles relies on the fact that they are the most likely to quickly evolve into diverse dynamical families: e.g., in the solar system, particles reaching the direct influence of Neptune could evolve into the scattered disk and all the way down into short-period comets (Levison & Duncan 1997).

These two limits separate the particles that have not been meaningfully affected (regions “a”), from those that have been significantly heated but have not reached the gravitational influence of the giant planet (regions “b”), and from those that have reached the gravitational influence of the giant planet (region 4).

We established a third set of limits from the two stronger MMRs present in the  $a_p$  vs.  $e_p$  plane considered here, namely the 3:2 and 2:1 MMRs with the giant planet. We define a region limited by  $\pm 0.7$  au at the nominal position of the resonances, this is, between 38.7 and 40.1 au, for the 3:2 MMR, and between 47.0 and 48.4 au, for the 2:1 MMR. We adopted this limit following the approach of Tiscareno & Malhotra (2009), who consider a particle to be potentially resonant if its semimajor axis remains within such interval; this width is overgenerous to be sure to include all resonant particles. Those regions are labeled as region 2 and 3, for the 2:1 and 3:2 MMRs, respectively (where 2a and 2b, as well as 3a and 3b regions are labeled depending on the  $e_{lim}$  defined above). We consider that particles belong to these resonant regions as long as their periastron is larger than that of the crossers, or equivalently, while they remain below the lower dot-dashed green line of the figure.

Finally, we define region 1 as the region outside the resonances, and below the limit of the crosser particles. Those regions are labeled 1a, 1xa, and 1xxa, for the particles below  $e_{lim}$ , and 1b, 1xb, and 1xxb for particles above  $e_{lim}$ .

From Fig. 3 we observe that the giant planet alone

cannot produce any significant perturbation on the disk, as expected, even after 1 Gyr. At the end of the simulation, only five particles have grown their  $e_p$  above  $e_{lim}$  through resonant perturbations at the 2:1 MMR of the giant. Not a single crosser is obtained for this case (neither at the end nor at any intermediate stage).

### 3. RESULTS AND DISCUSSION

In this work we explore the evolution of cometary nuclei in a cold debris disk under the gravitational influence of an interior giant planet and a distribution of DPs. In this scenario resonances are the most influential dynamical feature, but the dynamical evolution resulting from the interaction with the DPs will lead some particles, originally located away from the MMRs of the giant planet, into getting trapped in such resonances; in fact we find that this combination (DPs plus resonances) is much more influential than the resonances alone (as can be seen from the reference simulation). In other words, we are interested on the dynamical paths that replenish the giant's MMRs with cometary nuclei.

Due to computational constraints, we study the effect of a single configuration of DPs along the disk. Other distributions will lead to different individual fates of the particles in the disk, however, in a statistical sense, we do not expect the rate of particle resupplying to the MMRs to change significantly with different DP configurations. For this reason, we focus on the exploration of the most important parameter, in this case, the total mass of the DP distribution (equivalently, the mass of the debris disk).

To test the validity of the previous statement, we have explored one case with a disk of  $0.05M_{\oplus}$  (using only 2000 test particles), where we have moved one of the two most massive DPs (the one closer to the 2:1 MMR; see Figures 1 and 2) to an outer location on the disk. This is done for two reasons: one, it lets us explore the evolution of the disk with a significantly different spatial distribution of the mass, as we move the second largest DP, and two, it lets us test if the evolution and number statistics of cometary nuclei close and inside the 2:1 MMR is severely affected by this single massive planet. The results of this case are shown in Section 3.4.

#### 3.1. Evolution on the $a_p$ vs. $e_p$ plane

Fig. 4 shows the first sets of data points (cyan dots) and the last sets of data points (orange dots) of test particles in the plane  $a_p$  vs.  $e_p$ , for all the six different total masses of the DP distributions considered in this study. From panel 4a to panel 4f the masses are 0, 0.01, 0.0223, 0.05, 0.1118, and  $0.25M_{\oplus}$ . Note that the cyan dots do not represent the orbital parameters at  $t = 0$  but rather they represent the average over the first ten Myr, hence the cyan distributions will not be identical in the six panels.

A disk with a mass equal to  $0.01M_{\oplus}$ , added in the form of 50 DPs, is enough to have an impact on the dynamics of the debris disk, as seen in Fig. 4b. The presence of a mass similar to that of the smaller estimates of the mass of the CKB does not overheat the disk, however, we found that almost 13 times more particles are stirred into region 2b; this is even able to produce 19 crossers in 1 Gyr, as well as six particles in region 1b, excited by close encounters with the DPs alone. In order to illustrate this

behavior, in Fig. 5 we plot the evolution of the eccentricity for four of the particles initially located in region 1a which end up the simulation at region 1b. Those particles get their eccentricity stirred very quickly, in some cases after a single very close encounter with a DP, e.g. the red particle of Fig. 5 suffered an encounter with a minimum approximation distance,  $d_{min}$ , of just 9 411 km with a DP of mass equal to  $0.0022 M_{\oplus}$  (approximately the mass of Pluto); on the other hand, a series of close encounters, as close as  $d_{min} \sim 5.9 \times 10^5$  km, with several DPs in a short time-span, typically of the order of 1 to 5 Myr, can quickly stir the eccentricities, as is the case for the blue, green, and brown particles in Fig. 5.

Resonant particles increase their eccentricities by a completely different mechanism. In Fig. 6 we show the evolution of eccentricity and semimajor axis for four of the crosser particles that reach region 4 through the 2:1 MMR with the giant. These particles stir their eccentricities and inclinations chaotically (Tiscareno & Malhotra 2009), while maintaining a relatively bound semimajor axis. The semimajor axes variations are related to the amplitude of libration of the corresponding resonant argument. The larger those amplitudes, the less tightly trapped in the resonance particles are, thus they are able to escape more easily from the resonant region. From Fig. 6 we can see how large eccentricities are correlated to large variations of the semimajor axis of the resonant particles. The slow process that leads to the growth of the orbital elements and consequently to the escape of resonant particles is called chaotic diffusion.

In the trans-Neptunian region of the solar system, the slow chaotic diffusion that lets particles evolve from MMRs into scattered disk objects, Centaurs, and short-period comets, has been studied elsewhere (Duncan et al. 1995; Morbidelli 1997; Tiscareno & Malhotra 2009). Previous studies have focused on the slow chaotic diffusion originated by the overlapping of secondary resonances, such as secular and Kozai resonances (Duncan et al. 1995; Morbidelli et al. 1995; Morbidelli 1997). This phenomenon is independent of the presence or absence of large DPs close or even trapped inside the MMRs, at least for small disk masses; for example, Tiscareno & Malhotra (2009) show that the inclusion of Pluto, in the 3:2 MMR with Neptune, changes the mean particle lifetime inside the resonance by only 3% for 1 Gyr long integrations (when compared with a model without Pluto). In Section 3.4 we address this result by exploring the presence or absence, close to the 2:1 MMR, of a DP larger in size than the Moon (for a disk of  $0.05M_{\oplus}$ ), finding statistically equivalent results for the number and evolution of resonant particles.

While increasing the mass of the disk, the global behavior of particles is analogous to the previous  $0.01M_{\oplus}$  case, but it grows monotonically as a function of the mass of the disk (Muñoz-Gutiérrez et al. 2017), for example for masses of 0.0223 and  $0.05 M_{\oplus}$  (panels 4c and 4d), the crosser particles are still overwhelmingly produced inside the 2:1 MMR. Actually, only two non-resonant crossers are produced in the  $0.05M_{\oplus}$  disk (see panel 7d ahead). On the other hand, a new family of particles that approaches the giant planet, not through resonances, appears; these particles are not protected by the resonant mechanism and thus are prone to be affected by close

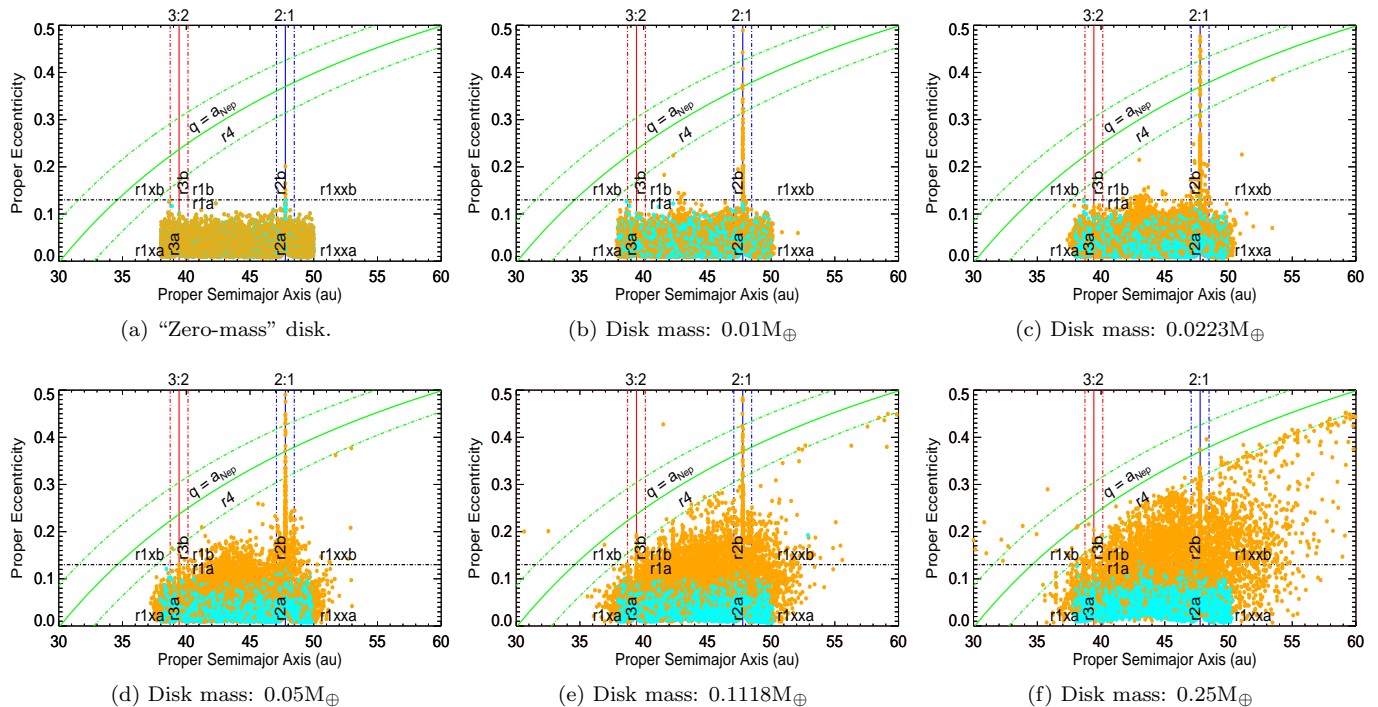


**Figure 4.** Initial and final point distributions of disk particles’ proper semimajor axes and eccentricities, as a function of disk mass.

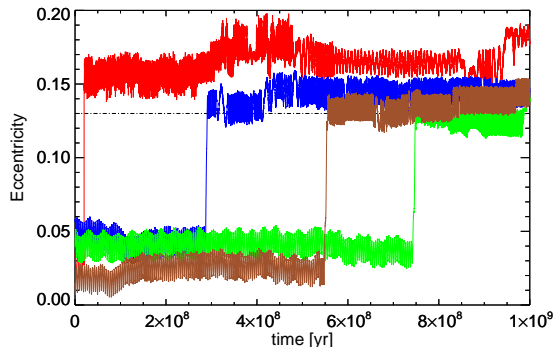


**Figure 5.** Eccentricity evolution of four region 1 particles, which are perturbed and stirred by close encounters with DPs. The black dot-dashed line indicates  $e_{lim}$ .

encounters with the giant planet and sent to larger semimajor axes while maintaining a short periastron, giving origin to a scattered population, similar to the scattered disk in the solar system (Gladman et al. 2008).

When the mass of the disk equals 0.1118 and 0.25  $M_{\oplus}$  (panels 4e and 4f) the effect of DP perturbations is more drastic. Now several crossers can reach very small periastrons even outside of resonances while the scattered population grows significantly. Interestingly, the 2:1 resonant crosser population, seems no longer protected from encounters with the giant when the mass of the disk is equal to 0.25 $M_{\oplus}$ . This implies that a larger fraction of the particles are sent into the scattered disk before they can reach smaller periastrons, or larger eccentricities. The stronger perturbations produced by more massive DPs increase the amplitude of libration of resonant particles, making them less tightly bound to the resonance, thus easily being ripped from it. This mechanism is analogous to the one originally proposed by Ip & Fernandez (1997) as the escape pathway of Plutinos in the solar system that contributes to the re-population

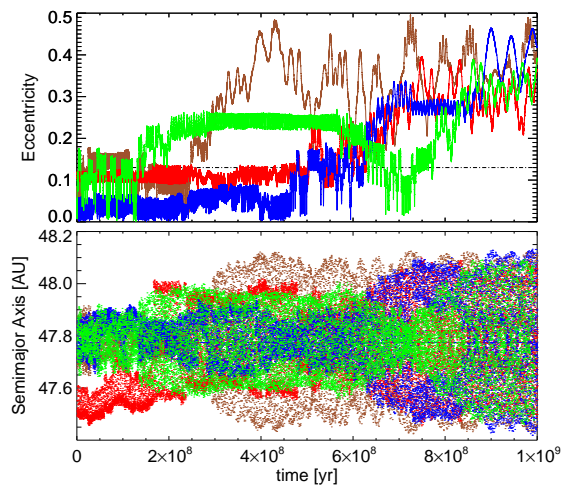


**Figure 6.** Eccentricity (top) and semimajor axis (bottom) evolution of four 2:1 resonant particles that become crossers before the end of the 1 Gyr simulation. The black dot-dashed line in the upper panel indicates  $e_{lim}$ , while the solid blue line indicates the center of libration of the 2:1 MMR.

of short-period comets. Indeed, Ip and Fernandez focus on the evolution of cometary nuclei inside Neptune’s 3:2 MMR into short-period comets, which were gravitationally scattered by hypothetical massive objects (with diameter in the range 100-500 km) located outside the 3:2 resonance.

Regarding the particles in region 1, where most disk particles reside, they are dynamically heated, with increasing eccentricity as a function of disk mass. We have studied this effect in a previous paper (Muñoz-Gutiérrez et al. 2017), as well as the stabilizing effect induced by the giant planet below a threshold disk mass (a giant like Neptune, will help stabilize the eccentricities of particles in the disk, if the mass in DPs is less than 0.096 $M_{\oplus}$ );

above this limit, the giant contributes to the dispersion of the particles. This effect can be seen as the rapid thickening of the disk in the last two panels of Fig. 4, which are above said threshold.

### 3.2. Origin of the “crosser” population

We are interested in the relation between the number and strength of the perturbations suffered by resonant particles inside MMRs as a function of the mass of the disk, or equivalently, as a function of the mass of the perturbing DPs; particularly for those particles within the 2:1 MMR.

In this work we focus on the fraction of cometary nuclei evolving towards, and inside, the two stronger MMRs of the region. In Figure 7 we show the paths of crosser particles in the  $a_p$  vs.  $e_p$  plane, for all the disks masses explored. We include the zero mass panel for completeness (panel 7a), as no crosser is produced by the giant planet’s perturbation alone.

As we did in Figure 4, we increase the mass from panel 7b to panel 7f, corresponding to 0.01 to 0.25  $M_{\oplus}$ . From Figure 7 we can see how most of the crossers come from the 2:1 MMR. Panel 7b corresponds to the lowest estimation for the mass of the CKB; here, all 19 observed crossers are produced within the 2:1 MMR, and all of them come from the neighborhood of the resonance. Interestingly, no crosser is produced from the 3:2 MMR, even after 1 Gyr. This result cannot be compared directly to other solar system studies due to the homogeneous density of our simulation; in the case of the solar system, the main MMRs with Neptune, in particular the two stronger resonances, 2:1 and 3:2, become overpopulated during the outer migration of Neptune, with the consequent resonant sweeping of all the region interior to the present location of the resonances (e.g. Malhotra 1993); thus, from the comparatively large number of resonant objects in the current Plutino population, one can expect a larger rate of escapees from this resonance, as observed in previous works (e.g. Morbidelli 1997; Tiscareno & Malhotra 2009). It is interesting to note that, although the number of particles near and inside the 2:1 MMR in our work is essentially the same as in the 3:2 MMR (region 2a vs. region 3a, see also panel a of Figure 10), the effectiveness of the 2:1 resonance in producing crosser particles is much higher; this is consistent with the results for the solar system of Nesvorný & Roig (2000, 2001), where particles with low eccentricity inside the 2:1 MMR with Neptune turn out to be unstable. In light of this result, even the relatively small population of twotinos in the Kuiper belt should be of importance as a source of new scattered objects that could become short-period comets.

Panel 7c shows similar results than the previous one, with a slight increase in the width, in the proper elements plane, of the region from where crosser particles originate; this region is still inside the 0.7 au we used to define region 2; there is also an increase in the number of crosser particles from 19 to 42. In panel 7d we note an important new behavior: while still most crossers evolve through the 2:1 MMR, now six particles from region 1 (plus one from region 3a) are stirred by close encounters with DPs, overcoming the crossers limit and, by not being protected by a resonance, they are immediately and strongly perturbed by the giant, sending them to

the scattered disk with large semimajor axis, or to the inner planetary system (see purple particle originating from region 1a). Another crucial aspect, that becomes evident in panel 7d, is the widening of the “source region” of particles that evolve towards the 2:1 MMR. Now particles originally located even at  $\sim 2$  au away from the resonance location, evolve into a resonant orbit, greatly increasing their eccentricities, enough to become crossers. We further illustrate this behavior in Fig. 9, where we show the semimajor axis evolution of four particles that started the simulation away from the 2:1 MMR libration center, which are sent to resonant orbits after some time. This mechanism, properly a resupplying of particles to the resonant region, is a direct product of the perturbations produced by massive DP objects, ranging in size, in this case (disk of mass equal to 0.05 $M_{\oplus}$ ), from a bit larger than Ceres to slightly larger than the Moon.

Panels 7e and 7f correspond to disks with masses where the giant planet no longer acts as stabilizer (Muñoz-Gutiérrez et al. 2017), therefore the dispersion observed in those panels grows significantly when compared to the first four panels, with particles which come from region 1 being rapidly sent either to the scattered population or to the inner planetary system. In Fig. 8 we show a subset of crosser particle track paths (roughly 5% of the total) for the two most massive disks, in order to illustrate with more clarity the evolution of the whole population of crossers for those cases. We again observe how the 2:1 resonant particles cannot reach the region of small periastron with moderate semimajor axis when the mass of the disk is 0.25 $M_{\oplus}$ , but instead they are quickly sent either to the scattered population or to the inner planetary system, as if they were not protected by the resonant mechanism at all.

### 3.3. Fractional Evolution of the Populations

To quantify the diffusive effect of the DPs over the disk particle population, we track the evolution of the fraction of particles in each of the four defined regions, during the 1 Gyr simulations. The results are shown in the six panels of Fig. 10. As in previous cases, from panel 10a to panel 10f the mass of the disk increases from zero to 0.25 $M_{\oplus}$ .

The slope of the curves in all panels changes slowly with increasing mass of the disk. Panel 10a shows a constant fraction of particles for all regions, as expected from previous results. In panel 10b we notice a decrease in the fraction of resonant particles below  $e_{lim}$  (solid lines) in favor of resonant particles above  $e_{lim}$  (dot-dashed lines), particularly for the 2:1 resonant particles (blue curves). This trend continues in the following panels, while the total number of particles (dashed lines) in the resonant regions, both above and below  $e_{lim}$ , remains roughly constant for the 2:1 MMR; however, a slight increase in the total number of 2:1 resonant particles (dashed blue lines) is noticeable in some panels of Figure 10. In contrast, the total number of 3:2 resonant particles (dashed red-line) closely follows that of the 3:2 resonant particles below  $e_{lim}$  (solid red line), while the number of 3:2 resonant particles above  $e_{lim}$  (dot-dashed red line) does not grow significantly in any panel. This means that particles excited above  $e_{lim}$  through the 3:2 MMR are quickly scattered and are consequently lost to other families, while the whole population in this reso-

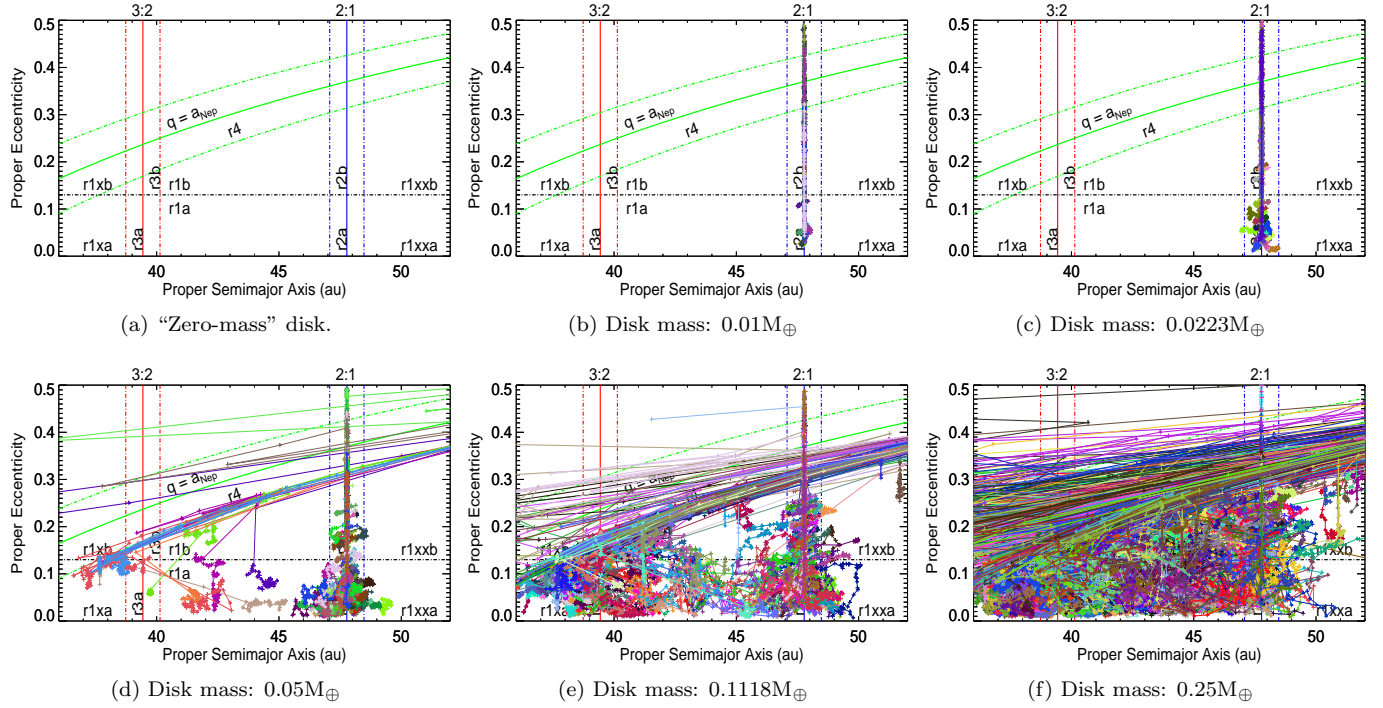


**Figure 7.** Track paths of all crosser particles in each simulation as a function of disk mass. The panels have 0, 19, 42, 70, 138, and 592 crossers respectively. The two most massive disks produce too many crossers to follow each particle individually. Each track that goes to the left of the panel represents a particle that visits the inner planetary system (at least briefly); each track that exits the panel to the right represents a particle that is scattered, either to the scattered disk or out of the system entirely.

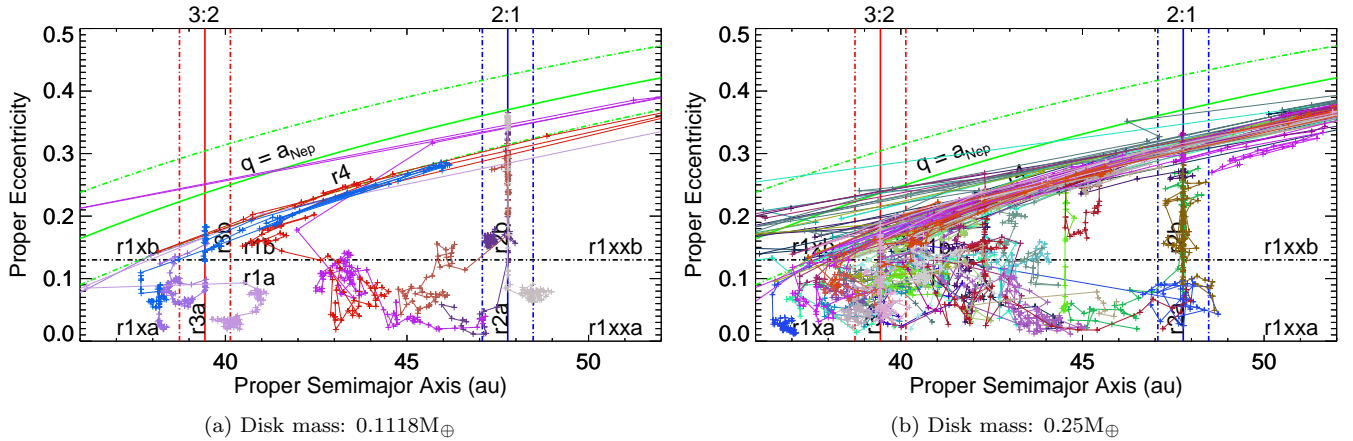


**Figure 8.** Same as panels 7e and 7f of Fig. 7, with only  $\sim 5\%$  of particle trajectories displayed for clarity. Left panel shows the track paths of 8 crossers while right panel shows 30 track paths.

nance gradually decreases.

The 2:1 total population is more or less constant during all the integration, but given that several particles are passed from the 2:1 resonance region above  $e_{lim}$  to the crosser population (solid green line), we can argue that an effective resupplying mechanism is operating in favor of the 2:1 MMR region, in order to maintain a steadily growing number of total region 2 particles while the crossers increase. Naturally, particles that resupply region 2 come from the neighborhood of the resonance (i.e. region 1; orange lines). Therefore, part of the decrease in the number of total region 1 particles (or non-resonant particles) occurs due to the resupplying of the 2:1 MMR. This trend is maintained below the stabiliz-

ing limit of the giant, this is, a decrease in the total number of non-resonant particles (dashed orange lines) is maintained until panel 10d, but in the last two panels we observe that the total number of non-resonant particles increases slightly. Therefore, above the stabilizing limit of the giant, a great number of particles from region 1a (solid orange lines) are excited towards region 1b (dot-dashed orange lines), while several others are sent towards the crosser region where they are scattered by the giant.

Regions 1, 2, and 4 increase their numbers with the increasing mass of the disk, while the only family that suffers a decrement in the number of particles is region 3, those of the 3:2 MMR. Even if those particles can-

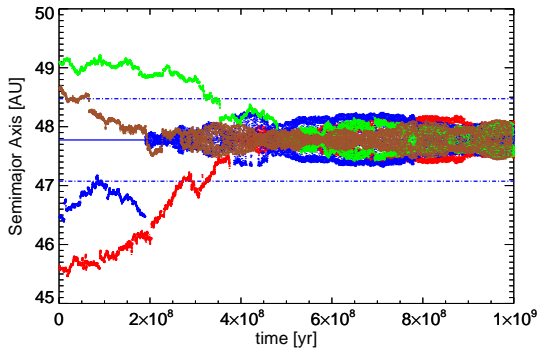


**Figure 9.** Semimajor axis evolution of four initially non-resonant particles that are sent to the 2:1 MMR region by perturbations from DPs. The solid blue line indicates the center of libration for the 2:1 MMR, while dot-dashed blue lines delimit our region 2.

not reach the crosser region through the 3:2 MMR, the majority of the perturbed particles coming from region 3 reach the scattered part of the disk, where they are counted as part of the 1b family. Finally, most of the crossers come originally from the 2:1 MMR region, with the second most abundant population of crossers coming from the 1a region (through the 1b region).

#### 3.4. The Crosser Production Efficiency of the 2:1 MMR is not a Result of a Single Large DP.

The relevance of these results would be greatly diminished if they changed dramatically with a different distribution of DPs. In this section we present results from a single smaller simulation of a disk with mass equal to  $0.05 M_{\oplus}$ , where we have exchanged the second largest DP of the distribution (the one closer to the 2:1 MMR in the rest of the simulations presented in this work) with one in the outskirts of the disk (beyond 50 au). All of the remaining characteristics of this simulation are the same as those described in Section 2. We will show that this simulation turns out to be statistically equivalent to our standard model.

In Figure 11 we compare the results of both of the  $0.05M_{\oplus}$  disk simulations. Our new simulation was done with 2000 particles; in Muñoz-Gutiérrez et al. (2017) we checked that simulations with that number of particles are statistically equivalent. Panel 11a shows the fractional number of particles evolution for all the regions described earlier, where the broad curves represent results from our standard simulation, while the thin curves are result from the modified simulation. The fractional number evolution in all regions is visually almost indistinguishable from one another, but with slightly larger fluctuations in the new, smaller, simulation.

Not surprisingly, regions 1 and 3 do not suffer any significant variation due to the position change of the large DP. We expect a larger difference close to the region previously affected by this object. In panel 11b we show a smaller region of the same plot shown in panel 11a, where only the fractional number evolution of regions 2, 3, and 4 are visible. In this scale, we observe that the fractional number of crossers is the same also for region 4 in both simulations. However, some differences for region 2 become evident in panel 11b.

Indeed, the broad blue curves (region 2 of the standard simulation) are, on average, slightly above the thin blue curves (region 2 in the modified simulation), however at

the end of the simulations, the large DP close to region 2 has been able to increase by  $\sim 13\%$  the fractional number of particles belonging to the 2:1 resonant region. Overall, a very small change for such extreme modification. This shows that the large quantity of objects that reach region 2b is more closely related to the behavior of the 2:1 resonance and not to the specific population of DPs in the initial seeding of our model.

Regarding the crossers, the influence of the large DP seems to be even smaller. Based on the previous results, we would not expect significant changes for other “statistically equivalent” DP configurations.

#### 3.5. Injection Rate of Ecliptic Comets in a Solar System Toy Model.

As a first specific example, we will use our toy model to try to determine if the mechanism introduced here (the injection of ecliptic comets due to the replenishment of giant’s MMRs by DPs) is relevant in the solar system. This is a preliminary estimation, a more detailed model is needed to obtain accurate results; we will study this problem in depth in a future work.

We recall that, although our simplified model cannot capture all the intricacies of the evolution of the Kuiper belt (e.g. important secular resonances produced by the presence of the other giant planets) an order of magnitude estimation is in place in order to motivate or discard the contribution of this mechanism in our planetary system.

As mentioned before, estimates of the mass of the CKB, vary between  $0.008M_{\oplus} < M_{CKB} < 0.06M_{\oplus}$  (Trujillo et al. 2001; Bernstein et al. 2004; Fuentes & Holman 2008; Vitense et al. 2010; Fraser et al. 2014), with most of them laying between  $0.01M_{\oplus} < M_{CKB} < 0.03M_{\oplus}$ ; since our generic disk does not limit itself to the cold component of the CKB nor accurately resemble the whole CKB (i.e. considering both the cold and hot components), we will proceed with the most conservative assumption in order to estimate the injection rate of comets in our solar system toy model, therefore we will make use of the results from our first disk mass simulation with  $M_{DPs} = 0.01M_{\oplus}$  (those who prefer larger masses can use the second or third masses presented in this work).

From panels 4b, 7b, and 10b we can see that the total number of crossers by the end of the simulation is 19. We have studied each of these 19 crossers to see if any is locked in a resonance and thus could be resonant protected against a direct encounter with the giant planet; we found that none of them is well trapped inside the resonance (i.e. the resonant argument does not consistently librate, but it changes regime from circulating to librating), therefore, given enough time, all of them will have a close encounter with the Neptune-like giant. We can now estimate that the rate at which particles reach the Neptune-like neighborhood, as a direct result of the resupplying mechanism induced by DPs, is  $\sim 4 \times 10^{-12} \text{ yr}^{-1}$ . In works from the literature, that consider the gravitational perturbations from the four giant planets of the solar system, the rate of escapes from the Kuiper belt region was found to be about 4 to  $6 \times 10^{-11} \text{ yr}^{-1}$  (Duncan et al. 1995; Levison & Duncan 1997; Volk 2013); our estimate is smaller by an order of magnitude. The same authors found that between 10-30% of particles would become short-period comets after they first

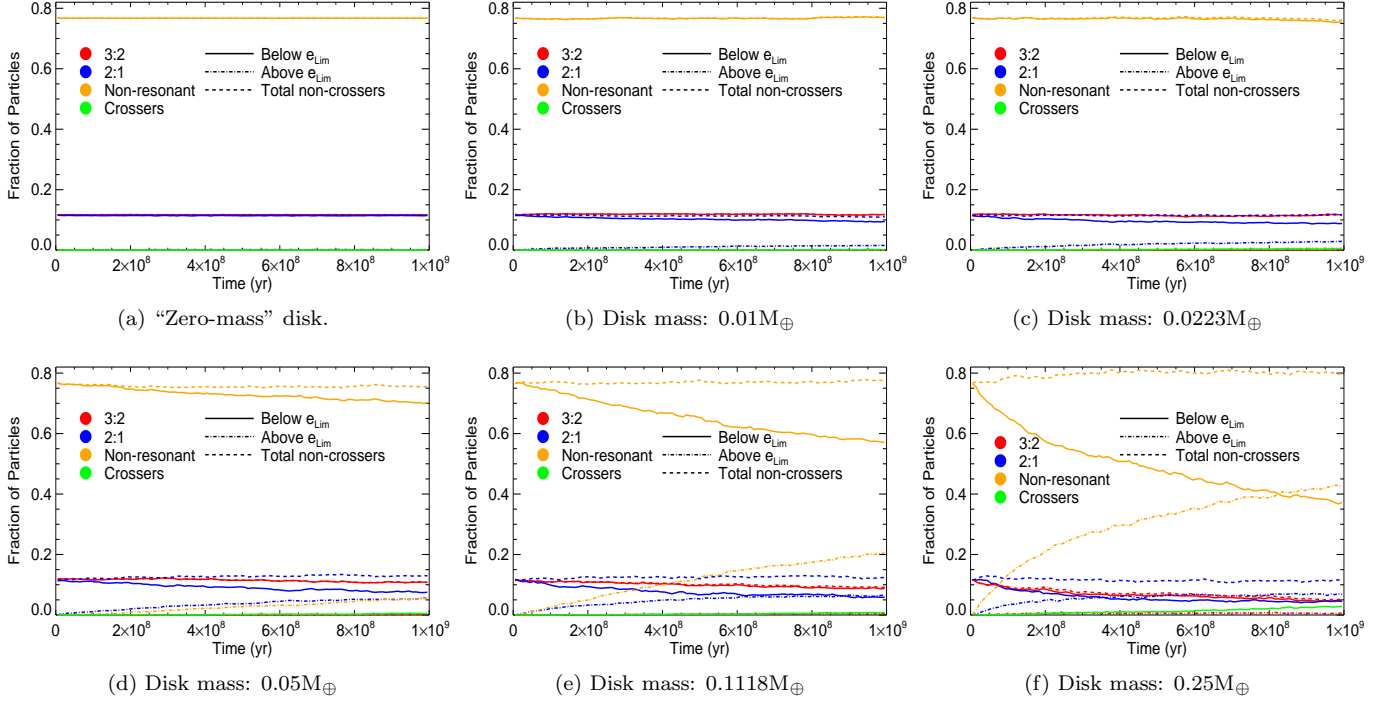


**Figure 10.** Fractional number evolution of the regions for all disk masses explored.

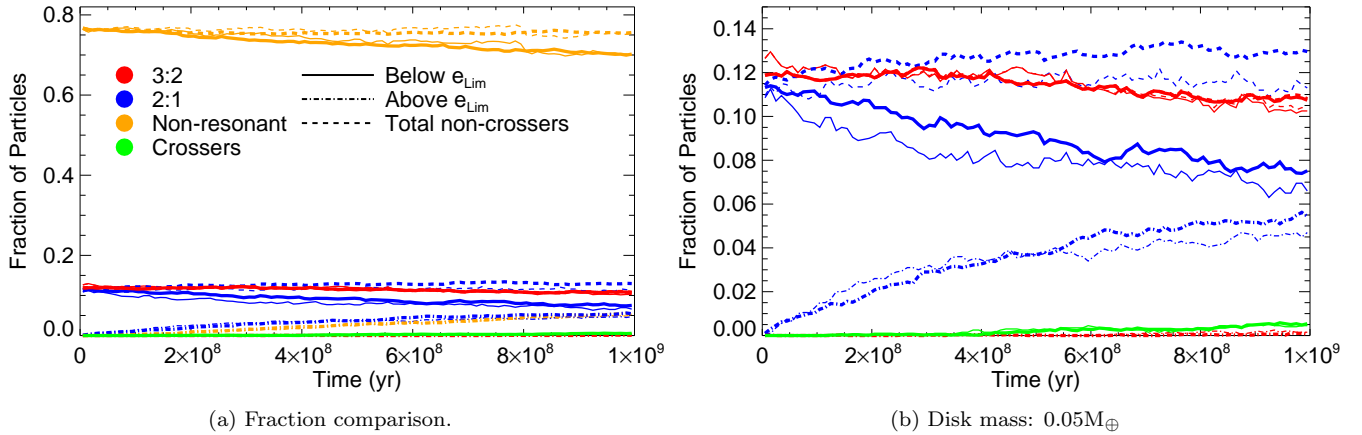


**Figure 11.** Comparison of the fractional number evolution for the simulations including 5000 (broad curves) and 2000 (thin curves) particles in a disk of  $0.05M_{\oplus}$ . Panel a shows the full range coverage as Figure 10, while panel b shows an amplified range in order to compare regions 2,3, and 4.

encounter Neptune, thus for our estimation we will use the middle value, 20%. Although in this work we are only considering one giant planet and a cold disk, the inclusion of more giant planets would increase the number of resonances in the belt, increasing in turn the number of regions that can be repopulated by the secular effect, and enhancing the efficiency of the DPs (probably only by a small factor).

In our scenario, the total injection rate of new comets to the inner solar system depends on the total number of cometary nuclei in the size range of  $\sim 1$  to 10 km, specifically located in the CKB, between  $\sim 38$  and 50 au. This number is not well constrained by observations due to the intrinsic faintness of such objects. Nonetheless, many authors have tried to estimate the required number of objects in the source region to account for the observed pop-

ulation of ecliptic comets, assuming it remains in steady state. Most works have focused on estimating the number of cometary objects in the scattered disk larger than  $\sim 2$  km, since the scattered disk is the dominant source of ecliptic comets for those models, finding that reservoirs in the range  $\sim 4.4 \times 10^8$  to  $\sim 6 \times 10^9$  cometary nuclei can account for the observed steady-state ecliptic comet population, depending on the model (e.g. Levison & Duncan 1997; Brasser & Morbidelli 2013; Brasser & Wang 2015; Nesvorný et al. 2017; Rickman et al. 2017). However, it is interesting to note that the most complete end-to-end simulations, those performed by Nesvorný et al., are still *anemic* when accounting for the population of large comets by at least a factor of two, unless an evolution size-dependent model is assumed.

Regarding the mass, several surveys suggest that the

mass of the scattered disk could be similar to that of the CKB or up to a few times more massive (Trujillo et al. 2001; Bernstein et al. 2004; Fuentes & Holman 2008; Vitense et al. 2010), with most of the values laying close to 1.5 times larger.

Regarding the population of cometary nuclei in the CKB: based on 4 Gyr simulations, Volk (2013) estimates that a source population of  $(1.7\text{-}3.5)\times 10^9$  objects larger than 1 km would be necessary to account for the number of Jupiter family comets (assuming steady state; if their only source was the CKB). Since the CKB accounts for approximately 40% of the combined mass of the CKB plus the scattered disk, we will assume  $(1.0 \pm 0.4) \times 10^9$  cometary sized objects in the CKB, in order to estimate the injection rate produced purely by the DP-induced resupplying mechanism in the solar system. This number is still below the most recent constraints set by occultation surveys (Schlichting et al. 2009; Bianco et al. 2010).

By the previous arguments, an order of magnitude injection rate can be estimated as the product of the precedent factors (number of objects in the CKB, times the rate of escapes through the resonances, times the fraction of particles that become short period comets after first encountering Neptune), therefore, the mechanism described here can potentially add a rate of  $7.6 \times 10^{-4}$  comets/yr, to previous theoretical expectations. As a point of reference, a recent estimation of the rate required to account for the population of visible Jupiter family comets is  $(8.4 \pm 1.7) \times 10^{-3}$  comets/yr (Rickman et al. 2017), therefore, the mechanism here proposed would account for  $\sim 9\%$  of such rate; this fraction depends on several quantities that are poorly understood, and can easily go from 5% up to 16% (the latter occurs if we take the upper limit for the number of cometary nuclei in the reservoir and the lower limit in the estimate in the injection rate of short period comets), but this number could be even as high as 50% if the mass of the CKB is larger than the one we assumed.

Also, recent discoveries of large TNOs (e.g. Bannister et al. 2016; Holman et al. 2017) show that the number of DP-sized objects in the trans-Neptunian region is of the order of a few tens and, even when most of new discoveries involve dynamically hot objects, such large bodies are still able to affect the population of a cold disk, as we have previously shown by Muñoz-Gutiérrez et al. (2017). We have looked for crossers in the 30 degree simulation from Muñoz-Gutiérrez et al., where we find that the efficiency drops by a factor of 2.1; however, the oblique encounters studied in that simulation are also similar to the interactions of the scattered disk with scattered DPs and thus, we can include the entire reservoir of cometary nuclei in the Kuiper belt that represents an increase of a factor of 2.5. Overall, this represents an increase of a factor of 1.18, when compared with our previous calculations. New members of the growing population of DP-sized objects in the solar system reaffirm the significance of the mechanism modeled here.

We do not claim this to be the rate at which new ecliptic comets are actually injected into the inner solar system. In fact, we would not be surprised if state of the art simulations of the solar system change this rate by a factor of two or more when compared to our generic model. Instead we show the potential importance of the mech-

anism proposed, besides the potential significance of the 2:1 MMR with Neptune as a source of new comets.

A complete and detailed numerical simulation, including all the four giant planets and the known trans-Neptunian DPs and largest objects, with an unbiased population of test particles that includes the diverse families of objects in the Kuiper belt, such as the cold CKB, the hot CKB, the scattered disk and the resonant populations, would be required to calculate accurately the injection rates of comets to the inner solar system. Such a simulation is beyond the scope of the present work.

### 3.6. Injection Rates of Ecliptic Comets in Extrasolar Systems

It is straightforward to extrapolate the existence of comets to extrasolar systems, specially considering that the exo-debris disks we know the best, such as the ones of Fomalhaut, Vega, HR4796,  $\beta$ Pictoris,  $\epsilon$ Eridani, and  $\tau$ Ceti, among others, are observed to be much more massive than our Kuiper belt. In fact, several studies have been presented already showing the highly likely presence of bodies from Ceres-size DPs to exo-comets in many systems (e.g. Weaver et al. 1995; Movshovitz et al. 2012; Bodman & Quillen 2016; Rappaport et al. 2018; Wyatt et al. 2018). In the near future, we will be able to study in a more statistical fashion processes that take comets to the inner planetary systems as we do now for the Kuiper belt.

The injection of comets to the inner part of extrasolar systems has been explored as a mechanism to explain the observed exozodiacal clouds (Bonsor et al. 2012), which are thought to result from starlight re-radiated by dust remnants of exocomet tails (analogous to the way the inhomogeneities observed in the solar system Zodiacal Cloud are believed to originate from comet tails residuals). Also, from an astrobiological point of view, the number of comets in young planetary systems can be critical as they constitute a potential risk for the habitability of rocky exoplanets, inside the narrow region where life can develop.

Massive exoplanetary debris belts (some of which are observed to be orders of magnitude more massive than the one in the solar system) could contain larger numbers of cometary-sized objects; this, combined with their larger mass in DPs, even larger than those explored in this work, would elevate the significance of the resupplying mechanism for those systems.

In the case of our most massive disk,  $0.25M_{\oplus}$ , the number of crossers at the end of the simulation is 592, which means that the rate at which particles reach the giant neighborhood is as much as  $\sim 1 \times 10^{-10} \text{ yr}^{-1}$ . From this and assuming similar conditions as for the the solar system (i.e. roughly 20% of the escaped particles reaching the stage of ecliptic comets) and a number of objects in the debris disk 25 times larger than what we assumed for the CKB (i.e.  $\sim 2.5 \times 10^{10}$ ), the injection rate turns out to be around 0.6 comets per year.

Naturally, the rate at which particles are passed from the outer system to the inner region will depend on the detailed configuration of giant planets in the system. For example, Bonsor & Wyatt (2012) have shown that the giant planets of the solar system are close to the optimal distribution in mass as well as spatially, to maximize the transfer rate of comets to the inner planetary system;

this means that the  $\sim 20\%$  efficiency used earlier could be an overestimation for extrasolar systems.

Again, we do not claim this to be a number representative for any particular system, but we show the importance of the resupplying mechanism induced by DP-sized objects in driving the otherwise stable particles into perturbed orbits, which could then become scattered by a giant planet. Also, we argue that the modeling of debris disks should consider the population of DP-sized objects if the secular dynamical effects are expected to be accounted for accurately.

#### 4. CONCLUSIONS

In this work we have explored a previously unstudied secular dynamical mechanism operating on debris disks: one induced by the presence of dozens of DP sized objects, that can potentially drive new cometary material into the strongest mean motion resonances of an interior giant planet. Once trapped in such resonances, the cometary nuclei can be destabilized either by slow chaotic diffusion or by a combination of this effect and perturbations from nearby massive DPs. The perturbed cometary nuclei have their eccentricities stirred enough to encounter the giant, potentially being sent into other dynamical families, such as a component analogue to the scattered disk or all the way down into the inner planetary system, where they would become ecliptic comets (given that their initial inclination is small).

The full dynamical path, from cometary nucleus in a debris disks to ecliptic comet, that we are introducing here, consists of several stages that can be summarized as follows

1. Replenishment: the repopulation of cometary nuclei into the resonances due to the secular interaction with DPs.
2. Stirring: the initial growth of the eccentricity (beyond  $e_{lim}$ ) due to the resonant effect of the giant planet.
3. Crossers: the eccentricity continues growing until the periastron is comparable to the giant planet's orbit.
4. Direct interaction: after the first time that the cometary nucleus closely approaches the giant planet, it can severely change its path inwards or outwards.
5. Cascade: cometary nuclei going inwards can potentially interact with other interior giant planets.
6. Short period Comets: A few of the cometary nuclei will get stabilized by the most interior giant planet in cometary orbits of short period with almost constant Tisserand parameter.

In this work, we have explored in detail the evolution of particles from stage 1 to stage 3, enough to demonstrate the proof of concept we are introducing in this work. Although stage 4 can be seen in the two most massive examples, in the lower mass examples it takes longer than 1 Gyr to set up and does not affect the proof of concept, furthermore, stages 5 and 6 strongly depend

on the specific planetary system under consideration, and those lay outside the scope of this paper.

In order to motivate further studies, we present predictions based on a toy model of the solar system, where we find this effect to be present. If we consider work from the literature to quantify the later stages (4 to 6), we find that with enough DPs in the solar system (DPs in the range size between Mimas and Pluto, assuming many of the smaller ones are still to be discovered), this mechanism would be able to contribute with around 9% of the injection rate of the new material required to sustain a steady-state population of ecliptic comets; this value depends on several poorly constrained quantities and can go from 5% up to 16%. Future dedicated surveys, like TAOS II that aims to characterize the population of the smaller bodies in the CKB (Lehner et al. 2016), will be of great importance to test these figures in detail.

In extrasolar systems, the destabilizing mechanism explored here may account for the population of comets that contribute to the existence of exozodiacal clouds. Also, if a large number of new comets are being injected to the inner parts of extrasolar systems, they can pose a threat to the habitability of inner rocky worlds. Such rates still need to be calculated for particular systems in which a debris disk is accompanied by one or more giant planets; but in our most massive scenario, the rate of new comets is estimated to be extremely large: around 0.6 comets per year. In young massive active systems, this number could be in accordance with events analogous to the late heavy bombardment in the early solar system.

We acknowledge an anonymous referee for useful comments. We acknowledge grant CONACyT Ciencia Básica 255167. AP acknowledges grant DGAPA-PAPIIT IN109716. We acknowledge the use of the *Atocatl* supercomputer at the Instituto de Astronomía of the Universidad Nacional Autónoma de México, where the simulations were performed.

#### REFERENCES

- Bannister, M. T., Alexandersen, M., Benecchi, S. D., et al. 2016, *AJ*, 152, 212
- Barr, A. C., & Schwamb, M. E. 2016, *MNRAS*, 460, 1542
- Bernstein, G. M., Trilling, D. E., Allen, R. L., et al. 2004, *AJ*, 128, 1364
- Bianco, F. B., Zhang, Z.-W., Lehner, M. J., et al. 2010, *AJ*, 139, 1499
- Bodman, E. H. L., & Quillen, A. 2016, *ApJL*, 819, L34
- Bonsor, A., & Wyatt, M. C. 2012, *MNRAS*, 420, 2990
- Bonsor, A., Augereau, J.-C., & Thébault, P. 2012, *A&A*, 548, A104
- Brasser, R., & Morbidelli, A. 2013, *Icarus*, 225, 40
- Brasser, R., & Wang, J.-H. 2015, *A&A*, 573, A102
- Chambers, J. E. 1999, *MNRAS*, 304, 793
- Dohnanyi, J. S. 1969, *Journal of Geophysical Research*, 74, 2531
- Dones, L., Brasser, R., Kaib, N., & Rickman, H. 2015, *Space Sci. Rev.*, 197, 191
- Duncan, M., Quinn, T., & Tremaine, S. 1988, *ApJL*, 328, L69
- Duncan, M. J., Levison, H. F., & Budd, S. M. 1995, *AJ*, 110, 3073
- Duncan, M. J., & Levison, H. F. 1997, *Science*, 276, 1670
- Fernandez, J. A. 1980, *MNRAS*, 192, 481
- Fraser, W. C., Kavelaars, J. J., Holman, M. J., et al. 2008, *Icarus*, 195, 827
- Fraser, W. C., & Kavelaars, J. J. 2008, *Icarus*, 198, 452
- Fraser, W. C., Brown, M. E., Morbidelli, A., Parker, A., & Batygin, K. 2014, *ApJ*, 782, 100

- Fuentes, C. I., & Holman, M. J. 2008, *AJ*, 136, 83
- Gladman, B., & Duncan, M. 1990, *AJ*, 100, 1680
- Gladman, B., Marsden, B. G., & Vanlaerhoven, C. 2008, *The Solar System Beyond Neptune*, 43
- Gulbis, A. A. S., Elliot, J. L., Adams, E. R., et al. 2010, *AJ*, 140, 350
- Holman, M. J., Payne, M. J., Fraser, W., et al. 2017, arXiv:1709.05427
- Ip, W.-H., & Fernandez, J. A. 1997, *A&A*, 324, 778
- Jewitt, D. 2018, *AJ*, 155, 56
- Lehner, M. J., Wang, S.-Y., Reyes-Ruiz, M., et al. 2016, *Proc. SPIE*, 9906, 99065M
- Levison, H. F., & Duncan, M. J. 1997, *Icarus*, 127, 13
- Levison, H. F., Duncan, M. J., Dones, L., & Gladman, B. J. 2006, *Icarus*, 184, 619
- Malhotra, R. 1993, *Nature*, 365, 819
- Matthews, B. C., Krivov, A. V., Wyatt, M. C., Bryden, G., & Eiroa, C. 2014, *Protostars and Planets VI*, 521
- Morbidelli, A., Thomas, F., & Moons, M. 1995, *Icarus*, 118, 322
- Morbidelli, A. 1997, *Icarus*, 127, 1
- Morbidelli, A. 2002, *Modern celestial mechanics : aspects of solar system dynamics*, by Alessandro Morbidelli. London: Taylor & Francis, 2002, ISBN 0415279399
- Muñoz-Gutiérrez, M. A., Pichardo, B., Reyes-Ruiz, M., & Peimbert, A. 2015, *ApJL*, 811, L21
- Muñoz-Gutiérrez, M. A., Pichardo, B., & Peimbert, A. 2017, *AJ*, 154, 17
- Nesvorný, D., & Morbidelli, A. 2012, *AJ*, 144, 117
- Movshovitz, N., Asphaug, E., & Korycansky, D. 2012, *ApJ*, 759, 93
- Nesvorný, D., & Roig, F. 2000, *Icarus*, 148, 282
- Nesvorný, D., & Roig, F. 2001, *Icarus*, 150, 104
- Nesvorný, D., & Vokrouhlický, D. 2016, *ApJ*, 825, 94
- Nesvorný, D., Vokrouhlický, D., & Roig, F. 2016, *ApJL*, 827, L35
- Nesvorný, D., Vokrouhlický, D., Dones, L., et al. 2017, *ApJ*, 845, 27
- Rickman, H., Gabryszewski, R., Wajer, P., et al. 2017, *A&A*, 598, A110
- Rappaport, S., Vanderburg, A., Jacobs, T., et al. 2018, *MNRAS*, 474, 1453
- Schlichting, H. E., Ofek, E. O., Wenz, M., et al. 2009, *Nature*, 462, 895
- Tiscareno, M. S., & Malhotra, R. 2009, *AJ*, 138, 827
- Trujillo, C. A., Jewitt, D. C., & Luu, J. X. 2001, *AJ*, 122, 457
- Vitense, C., Krivov, A. V., & Löhne, T. 2010, *A&A*, 520, A32
- Volk, K., & Malhotra, R. 2008, *ApJ*, 687, 714-725
- Volk, K. M. 2013, Ph.D. Thesis
- Weaver, H. A., A'Hearn, M. F., Arpigny, C., et al. 1995, *Science*, 267, 1282
- Welsh, B. Y., & Montgomery, S. L. 2018, *MNRAS*, 474, 1515
- Wyatt, M. C. 2008, *ARA&A*, 46, 339
- Wyatt, M. C., van Lieshout, R., Kennedy, G. M., & Boyajian, T. S. 2018, *MNRAS*, 473, 5286
- Wyatt, M. C. 2018, arXiv:1804.08636